TECHNISCHE MECHANIK
an open access journal

journal homepage: www.ovgu.de/techmech

Tech. Mech., Vol. 45, Is. 1, (2025), 31–45

Received: 21.10.2024
Accepted: 02.07.2025
Available online: 08.07.2025

Nonlinear thermal radiation, heat generation/absorption and chemical reaction effects on hydromagnetic Williamson nanofluid flow over a stretching sheet

Bharat Laxmi* and Khem Chand

Department of Mathematics & Statistics, H. P. U., Shimla, 171005, India

Abstract: In this paper, we have examined the two-dimensional flow of hydromagnetic Williamson nanofluid over a stretching sheet considering the effects of nonlinear thermal radiation, heat generation/absorption and chemical reaction.The governing equations are converted into nonlinear ordinary differential equations by using similarity transformations and solved numerically by the in-built function bvp4c in MATLAB software. Furthermore, the effects of the physical parameters such as Williamson parameter, Lewis number, Schmidt number, Prandtl number, magnetic field parameter, Darcy number and nanoparticle parameters (diffusivity ratio and heat capacities ratio) have been studied. The expressions for coefficients of skin friction, Nusselt number and Sherwood number have been derived and computed. The influence of various physical parameters on the velocity, temperature and concentration profile are presented with the help of graphs & tables and discussed.

Keywords: Hydromagnetic; Williamson nanofluid; Stretching sheet; Thermal radiation; Heat generation/absorption.

1 Introduction

A nanofluid is a fluid containing nanometer-sized particles (1-100nm), called nanoparticles. These fluids are engineered colloidal suspensions of nanoparticles in a base fluid. The nanoparticles used in nanofluids are typically made of metals, oxides, carbides, or carbon nanotubes. Common base fluids include water, ethylene glycol and oil. Nanofluids have novel properties that make them potentially useful in many applications in heat transfer, including microelectronics, fuel cells, pharmaceutical processes and hybrid-powered engines, domestic refrigerator, chiller, heat exchanger, in grinding, machining and in boiler flue gas for temperature reduction. In recent years, the study of non-Newtonian fluids has received the attention of researchers around the world due to its developments and their wide range of applications.The Williamson fluid is one of the most important non-Newtonian fluids characterized by less viscosity and high rate of shear stress and very similar in its properties to that of polymeric solutions. It has some real-life applications, such as simulating the extrusion and cooling of stretched sheets, which is crucial in the production of polymers and plastics because of non-Newtonian behavior and surface heating. It replicates magnetically targeted drug delivery and blood flow under chemical and thermal stimuli in biomedical engineering. The concept is extremely applicable to heat exchangers and solar energy systems. These models help design advanced nanofluid coolants under strong magnetic fields and thermal gradients in nuclear reactor cooling. Additionally, the interplay of heat sources, magnetic fields and chemical reactions in chemical and catalytic reactors promotes enhanced reaction control and process optimization. Finally, such research helps the glass and metal sectors better regulate heat in cooling and high-temperature sheet manufacturing operations.
In this advancement of technological world many researchers have been attracted by the flow and energy transfer of non-Newtonian fluid due to its fast technological applications in the field of manufacturing engineering processes such as food mixing and chyme movement in the intestine, flow of plasma, flow of mercury amalgams and lubrications with heavy oils and greases. Based on these numerous applications many studies are focussed on non-Newtonians fluid flow and heat transfer. A model discovered by Williamson (1929) introduce pseudoplastic materials and proposing a fluid model for non-Newtonian fluids, which was later known by his name. Khan and Pop (2010) investigated boundary layer flow of a nanofluid past a stretching sheet. The Buongiorno's model has been employed by Kuznetsov and Nield (2010) to investigate the effects of thermophoresis and Brownian movement on the natural convection flow in the presence of nanoparticles over a vertical plate. Ramesh et al. (2012) explained heat transfer in MHD dusty boundary flow over an inclined stretching sheet with nonuniform heat source/sink. Nadeem et al. (2013) were the first ones who developed the two-dimensional boundary layer equations for the flow of Williamson fluid past a stretching sheet. Sheikholeslami and Ganji (2014) investigated the three-dimensional heat and mass transfer in rotating system using nanofluid. Hussain et al. (2017) has studied the effects of viscous dissipation and Joule heating on MHD Sisko nanofluid over a stretching cylinder. However, free convective heat and mass transfer of MHD non-Newtonian nanofluids over a cone in the presence of a nonuniform heat source/sink was studied by Raju et al. (2016). Sajadifar et al. (2017) examined the fluid flow and heat transfer of non-Newtonian nanofluid in a microtube considering slip velocity and temperature jump boundary conditions. Khan et al. (2018) has studied viscosity of a Williamson nanofluid flow due to thermal and solutal stratification. Hayat et al. (2018) has described the mixed convective three-dimensional flow of Williamson nanofluid subject to chemical reaction. Hamid et al. (2019) has studied the multiple solutions for MHD transient flow of Williamson nanofluids with convective heat transport. Subbarayudu et al. (2020) investigated the assessment of time-dependent flow of Williamson fluid with radiative blood flow against a wedge.

* E-mail address: mahinegi456@gmail.com
doi: 10.24352/UB.OVGU-2025-039

The MHD flow properties of a Williamson nanofluid across an exponentially permeable stretching curved surface with varying thermal conductivity have been investigated by Ahmed et al. (2021). A study by Yousef et al. (2022) examined the effects of chemical reactions on MHD dissipative Casson-Williamson nanofluid flow through a porous medium over a slippery stretched sheet. The Williamson nanofluid flow across an exponentially stretching sheet with slip velocity was examined by Khader et al. (2023) using the spectral collocation approach. An MHD Williamson nanofluid flow across a nonlinear stretching sheet submerged in a permeable medium was examined by Kumar et al. (2024) to examine the impacts of cross-diffusion. Rao and Deka (2024) conducted a numerical simulation of the MHD hybrid nanofluid flow via a porous stretched sheet that emits heat radiation.
Motivated by above researches main objective of the present work is to examine the two-dimensional flow of hydromagnetic Williamson nanofluid over a stretching sheet under the influence of nonlinear thermal radiation, heat generation/absorption and chemical reaction effects. The distributions of velocity, temperature and concentration of Williamson nanofluids taking into account. The similarity transformations are used to convert the partial differential equations into nondimensional variables. Further, the governing system of ordinary differential equations has been solved numerically by the in-built function bvp4c in MATLAB software. Further the effects of different dimensionless parameters like Brownian motion parameter, thermophoresis coefficient, Williamson parameter, radiation parameter, Schmidt number, Prandtl number, magnetic field parameter, Darcy number and nanoparticle parameters (diffusivity ratio and heat capacities ratio) have been studied. The expressions for coefficients of skin friction, Nusselt number and Sherwood number have been derived and computed. The influence of various physical parameters over a velocity, temperature and concentration profile are presented with the help of graphs & tables and discussed.

Nomenclature

λ - Non-Newtonian Williamson parameter
θ - Dimensionless temperature
τ_w - Shear stress along stretching surface
D_T - Thermophoresis diffusion coefficient
g - Acceleration due to gravity
L - Characteristic length
B_0 - Constant applied magnetic field
R^* - Constructive reaction rate
T_w - Varying temperature of the surface
T_∞ - Free stream temperature
η - Dimensionless similarity variable
γ - Chemical reaction parameter
Nb - Brownian motion parameter
k-Thermal conductivity for fluid
$(\rho C_p)_f$ - Heat capacity of the base fluid
$(\rho C_p)_p$ - Heat capacity of a nanoparticle
D_B - Brownian diffusion coefficient
C - Nanoparticle volume fraction
M - Dimensionless magnetic field parameter
ϕ - Dimensionless concentration function
C_w - Nanoparticle fraction at wall
C_f-Local skin friction coefficient
Q - Uniform volumetric heat source/sink parameter
u - Velocity in x-direction
ψ - Stream function
v - Velocity in y-direction
u_w - Surface velocity
α - Thermal diffusivity
v_w - Wall mass transfer velocity
Γ - Time constant
T - Fluid temperature
α - Thermal diffusivity
Sc - Schmidt number
ρ - Density of the fluid
Nt - Thermophoresis parameter
K - Darcy permeability
θ_w - Ratio temperature
Pr - Prandtl number
ν - Kinematic viscosity
Da - Darcy number
R - Radiation parameter
Ec - Eckert number
Re_x - Local Reynolds number
Sh_x - Local Sherwood number
Nu_x - Local Nusselt number

2 Mathematical formulation

We consider the two-dimensional steady flow of an incompressible Williamson nanofluid over a stretching surface through a porous medium. A cartesian co-ordinate system with X-axis oriented horizontally and Y-axis oriented vertically upward through the origin is considered. According to the physical problem given in Fig. 1, u and v are the elements of velocity in x and y directions of the fluid respectively. The plate is stretched along the x-axis with the velocity $U_w(x)$=Bx, where $B > 0$ is the stretching rate. The fluid velocity, temperature and concentration of nanoparticle near surface are assumed to be U_w, T_w and C_w respectively. The governing two-dimensional boundary layer equations by following (Nadeem and Hussain (2014)) can be written as follows:

$$\frac{\partial u}{\partial x} + \frac{\partial v}{\partial y} = 0 \tag{1}$$

$$u\frac{\partial u}{\partial x} + v\frac{\partial u}{\partial y} = \nu\frac{\partial^2 u}{\partial y^2} + \sqrt{2}\nu\Gamma\frac{\partial u}{\partial y}\frac{\partial^2 u}{\partial y^2} - \frac{\sigma B_0^2}{\rho}u - \frac{\nu}{K}u \tag{2}$$

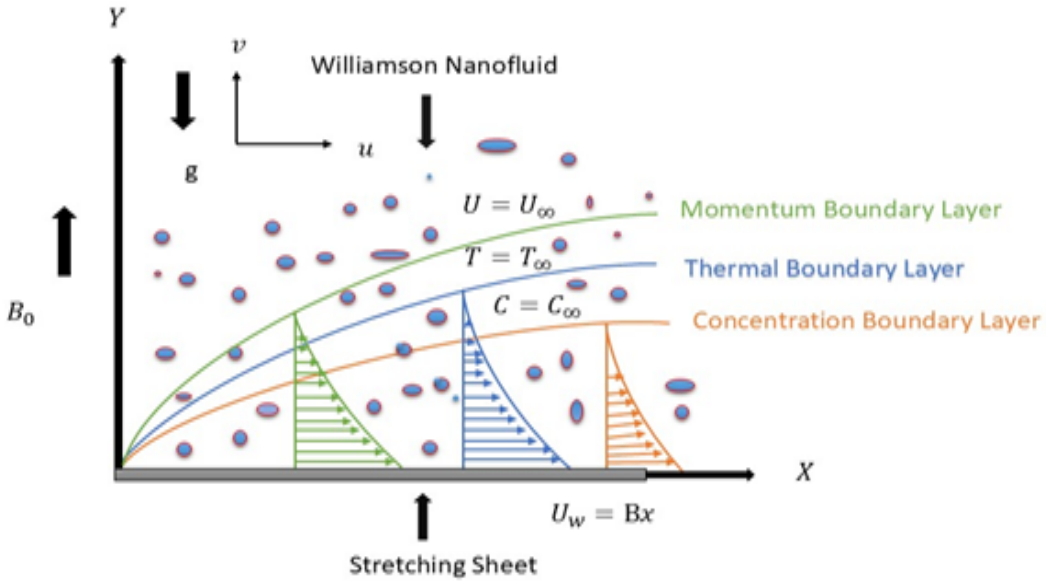

Fig. 1: Geometrical configuration of the physical model for stretching surface

$$u\frac{\partial T}{\partial x}+v\frac{\partial T}{\partial y}=\alpha\frac{\partial^2 T}{\partial y^2}-\frac{1}{(\rho c_p)_f}\frac{\partial q_r}{\partial y}+\frac{(\rho C_p)_p}{(\rho C_p)_f}\left[D_B\left(\frac{\partial C}{\partial y}\frac{\partial T}{\partial y}\right)+\frac{D_T}{T_\infty}\left(\frac{\partial T}{\partial y}\right)^2\right]+\frac{\sigma B_0^2}{(\rho C_p)_f}u^2+\frac{Q_0}{(\rho c_p)_f}(T-T_\infty) \tag{3}$$

$$u\frac{\partial C}{\partial x}+v\frac{\partial C}{\partial y}=D_B\frac{\partial^2 C}{\partial y^2}+\frac{D_T}{T_\infty}\frac{\partial^2 T}{\partial y^2}-R^*(C-C_\infty) \tag{4}$$

The associated boundary conditions are as follows:

$$\begin{aligned}&\text{at } y=0, \quad u=U_w,\ v=0,\ T=T_w,\ C=C_w\\ &\text{as } y\to\infty, \quad u\to 0,\ T\to T_\infty,\ C\to C_\infty\end{aligned} \tag{5}$$

where $U_w(x)=Bx$ represent the stretching surface velocity and $B>0$ is the stretching rate. Using Rosseland approximation for the radiative heat flux q_r from Eq. (3) we have

$$q_r=-\frac{4\sigma^*}{3k^*}\frac{\partial T^4}{\partial y}=-\frac{16\sigma^*}{3k^*}T^3\frac{\partial T}{\partial y} \tag{6}$$

where σ^* signifies Stefan-Boltzmann constant and k^* symbolizes Rosseland mean absorption coefficient. The radiative heat flux equation, then q_r given in Eq. (6) can be written as:

$$\frac{\partial q_r}{\partial y}=-\frac{16\sigma^*}{3k^*}\frac{\partial}{\partial y}\left(T^3\frac{\partial T}{\partial y}\right) \tag{7}$$

substituting Eq. (7) into Eq. (3), we get the transform energy equation as follows:

$$u\frac{\partial T}{\partial x}+v\frac{\partial T}{\partial y}=\alpha\frac{\partial^2 T}{\partial y^2}+\frac{16\sigma^*}{3k^*(\rho c_p)_f}\frac{\partial}{\partial y}\left(T^3\frac{\partial T}{\partial y}\right)+\frac{(\rho c_p)_p}{(\rho c_p)_f}\left[D_B\left(\frac{\partial C}{\partial y}\frac{\partial T}{\partial y}\right)+\frac{D_T}{T_\infty}\left(\frac{\partial T}{\partial y}\right)^2\right]+\frac{\sigma B_0^2}{(\rho c_p)_f}u^2+\frac{Q_0}{(\rho c_p)_f}(T-T_\infty) \tag{8}$$

Introducing the following similarity transformation to non-dimensionlize the given equations:

$$u=Bx'(\eta),\ v=-\sqrt{B\nu}\,f(\eta),\ \eta=\sqrt{\frac{B}{\nu}}\,y,\ \theta(\eta)=\frac{T-T_\infty}{T_w-T_\infty},\ \phi(\eta)=\frac{C-C_\infty}{C_w-C_\infty}. \tag{9}$$

where η is the similarity variable, $f(\eta)$, $\theta(\eta)$ and $\phi(\eta)$ represents the dimensionless stream velocity, temperature and concentration functions respectively of nanoparticles.

Since, $u = \frac{\partial \psi}{\partial y}$, $v = -\frac{\partial \psi}{\partial x}$ therefore the stream function $\psi(x, y)$ satisfies the continuity Eq. (1). The momentum and energy equations can be transformed into the corresponding ordinary non-linear differential equation by using non-dimensional variable as given in Eq. (9), the Eq. (2), Eq. (4) and Eq. (8) transforms to the following equations:

$$f''' - (f')^2 + ff'' + \lambda f'' f''' - Mf' - Daf' = 0 \tag{10}$$

$$\theta'' + R\left(1 + (\theta_w - 1)\theta\right)^3 \theta'' + 3R(\theta_w - 1)\left(1 + (\theta_w - 1)\theta\right)^2 (\theta')^2 + \mathrm{PrNb}\,\theta'\,\phi' + \mathrm{PrNt}\,(\theta')^2 + \mathrm{PrMEc}\,(f')^2 + \mathrm{PrQ}\,\theta + \mathrm{Pr}f\,\theta' = 0 \tag{11}$$

$$\phi'' + \mathrm{Sc}\,\phi' f - \mathrm{Sc}\gamma\phi + \frac{1}{Nb}\theta'' = 0 \tag{12}$$

where f, θ and ϕ are function of η and prime denotes derivatives to η.

The corresponding boundary conditions are given as

$$\begin{aligned} &\text{at } \eta = 0,\ f(0) = 0,\ f'(0) = 1, \theta(0) = 1, \phi(0) = 1, \\ &\text{as } \eta \to \infty, \quad f'(\eta) \to 0, \quad \theta(\eta) \to 0, \quad \phi(\eta) \to 0 \end{aligned} \tag{13}$$

where $\lambda = \Gamma x\sqrt{\frac{2B^3}{\nu}}$ is the non-Newtonian Williamson parameter, $M = \frac{\sigma B_0^2}{\rho B}$ is the magnetic field parameter, $Da = \frac{\nu}{kB}$ is the Darcy number, $R = \frac{16\sigma^* T_\infty^3}{3kk^*}$ is the nonlinear thermal radiation parameter, $\theta_w = \frac{T_w}{T_\infty} > 1$ is the ratio of temperature, $\mathrm{Pr} = \frac{\nu}{\alpha}$ is the Prandtl number, $\mathrm{Nb} = \frac{(\rho c_p)_p D_B (C_w - C_\infty)}{\nu(\rho c_p)_f}$ is the Brownian motion parameter, $\mathrm{Nt} = \frac{(\rho c_p)_p D_T (T_w - T_\infty)}{\nu(\rho c_p)_f T_\infty}$ is the thermophoresis parameter, $\mathrm{Ec} = \frac{U_w^2(x)}{(c_p)_f (T_w - T_\infty)}$ is the Eckert number, $Q = \frac{Q_0}{(\rho c_p)_f B}$ is the heat generation ($Q > 0$) or absorption ($Q < 0$) parameter, $\mathrm{Sc} = \frac{\nu}{D_B}$ is the Schmidt number and $\gamma = \frac{R^*}{B}$ is the chemical reaction parameter.

3 Some important characteristics of flow field

3.1 Local skin friction coefficient

$$C_f = \frac{\tau_w}{\rho U_w^2} \tag{14}$$

where τ_w is the surface shear stress along the stretching surface which is given by

$$\tau_w = \mu \left[\frac{\partial u}{\partial y} + \frac{\Gamma}{\sqrt{2}}\left(\frac{\partial u}{\partial y}\right)^2\right]_{y=0} \tag{15}$$

The local skin friction coefficient in terms of transformed variables Eqs. (9), (14) and (15) can be obtained as

$$(\mathrm{Re}_x)^{1/2} C_f = \left[f'' + \frac{\lambda}{2}(f'')^2\right]_{\eta=0} \tag{16}$$

3.2 The dimensionless coefficient of heat transfer (Nusselt number)

The dimensionless expression for the local Nusselt number is given by

$$\mathrm{Nu}_x = \left[\frac{x q_w}{k(T_w - T_\infty)}\right]_{y=0} \tag{17}$$

$$\text{where } q_w = \left[-k\frac{\partial T}{\partial y} + q_r\right]_{y=0} \quad \text{and} \quad q_r = \left[-\frac{16\sigma^*}{3k^*} T^3 \frac{\partial T}{\partial y}\right]_{y=0}. \tag{18}$$

The dimensionless expression for local Nusselt number in terms of transformed variables Eq. (9) and using Eq. (17) & Eq. (18) turned out to be

$$(\mathrm{Re}_x)^{-\frac{1}{2}} \mathrm{Nu}_x = -\left[1 + R\left(1 + (\theta_w - 1)\theta\right)^3\right]\theta'(0). \tag{19}$$

3.3 The dimensionless coefficient of mass transfer (Sherwood number)

The dimensionless expression for local Sherwood number is given by

$$\mathrm{Sh}_x = \left[\frac{-x}{C_w - C_\infty}\frac{\partial C}{\partial y}\right]_{y=0} \tag{20}$$

The dimensionless expression for local Sherwood number in terms of transformed variables Eq. (9) and using Eq. (20) turned out to be

$$(\mathrm{Re}_x)^{-\frac{1}{2}}\,\mathrm{Sh}_x = -\phi'(0) \tag{21}$$

4 Results and Discussion

In this paper we have obtained the effects of non-linear thermal radiation heat generation/absorption and chemical reaction on hydromagnetic Williamson nanofluid flow and a numerical solution for nanofluid velocity, temperature and concentration is obtained to describe the nature of Williamson fluid flow towards a stretching surface. Keeping this in mind, we discuss the numerical results in terms of non-dimensional velocity, temperature and nanoparticles concentration for different governing parameters, non-Newtonian Williamson parameter (λ), magnetic field parameter (M), Darcy number (Da), thermal radiation field parameter (R), Prandtl number (Pr), Brownian motion parameter (Nb), thermophoresis parameter (Nt), Eckert number (Ec), heat generation/absorption parameter (Q), Schmidt number (Sc), chemical reaction parameter (γ) and temperature ratio parameter (θ_w). We use bvp4c solver in MATLAB software to obtain numerical solutions and plotted graphs.

4.1 Impact on velocity profile $f'(\eta)$

The influence of the magnetic field parameter (M) on the dimensionless velocity $f'(\eta)$is shown in Fig. 2. It is observe that increasing values of the magnetic field parameter retard the velocity at all points of the flow field. From Fig. 3. it is observe that for a nanofluid the velocity as well as the boundary layer thickness reduces with increase in the non-Newtonian Williamson parameter (λ). It is observed from Fig. 4. that the velocity decreases with large value of Darcy number (Da). When the Darcy number increases, the inertial forces become more dominant and the viscous forces become less dominant. This results in a decrease in the velocity of the fluid flow. Therefore, the velocity of the fluid flow decreases with an increase in the Darcy number.

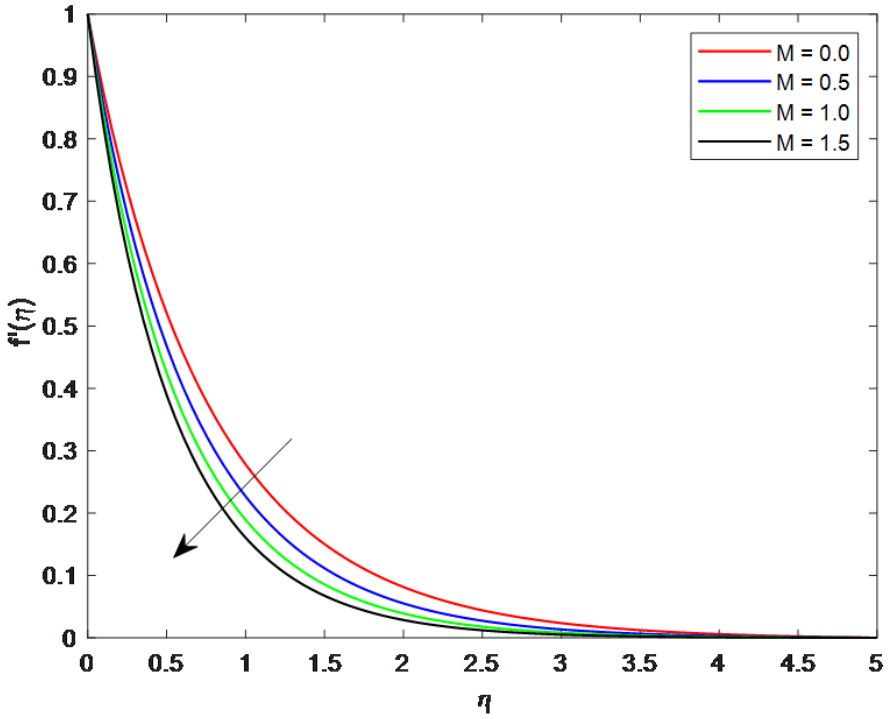

Fig. 2: Velocity profiles $f'(\eta)$ for various values of magnetic field parameter M when $Nb = 0.5$, $Nt = 0.5$, $Pr = 5$, $Sc = 2$, $\lambda = 0.2$, $Da = 0.5$, $Q = -0.1$, $Ec = 0.4$, $R = 0.5$, $\theta_w = 1.2$, $\gamma = 2.5$.

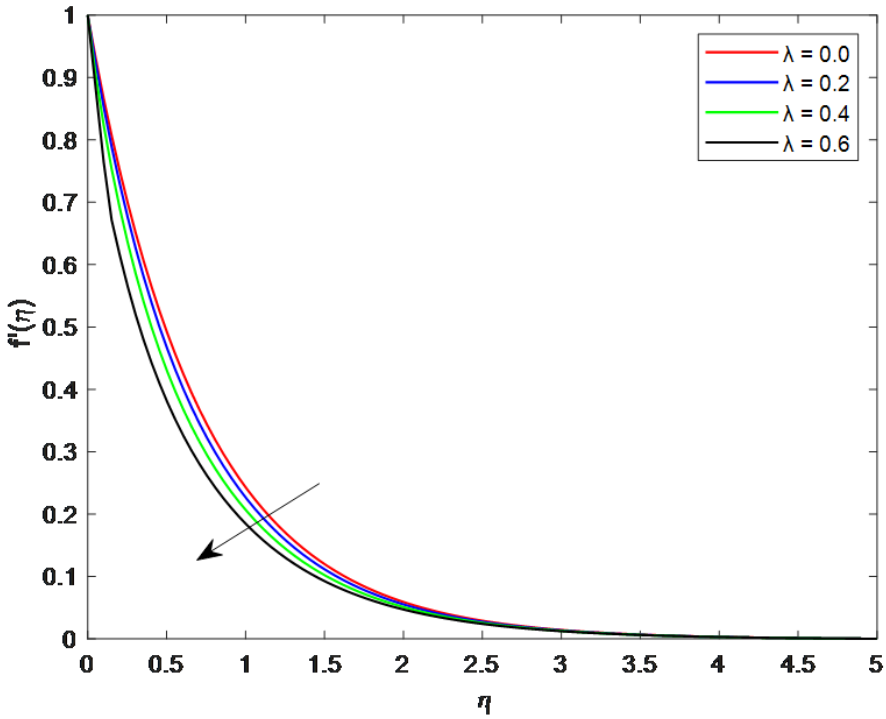

Fig. 3: Velocity profiles $f'(\eta)$ for various values of non- Newtonian Williamson parameter λ when $Nb = 0.5$, $Nt = 0.5$, $Pr = 5$, $Sc = 2$, $M = 0.5$, $Da = 0.5$, $Q = -0.1$, $Ec = 0.4$, $R = 0.5$, $\theta_w = 1.2$, $\gamma = 2.5$.

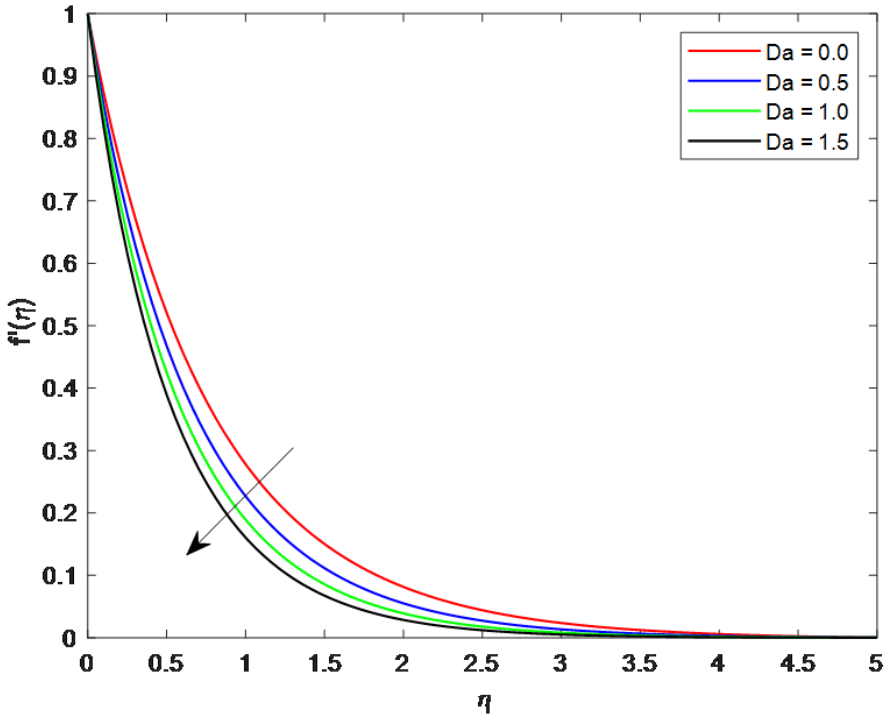

Fig. 4: Velocity profiles $f'(\eta)$ for various values of Darcy number Da when $Nb = 0.5$, $Nt = 0.5$, $Pr = 5$, $Sc = 2$, $M = 0.5$, $\lambda = 0.2$, $Q = -0.1$, $Ec = 0.4$, $R = 0.5$, $\theta_w = 1.2$, $\gamma = 2.5$.

4.2 Impact on temperature profile $\theta(\eta)$

Fig. 5. shows that with an increase in the Prandtl number (Pr) the temperature $\theta(\eta)$ decreases. An increase in the Prandtl number reduces the thermal boundary layer thickness. When Pr is small, heat diffuses quickly compared to the velocity. The impact of the Brownian motion parameter (Nb), on temperature $\theta(\eta)$ has been shown in Fig. 6. From the figure we found that the enhancement of Brownian motion parameter the dimensionless temperature increases. Brownian motion is caused by the random collisions of the particles with other particles in the fluid. Physically, it is noted that the different nanoparticles have different Brownian motions,

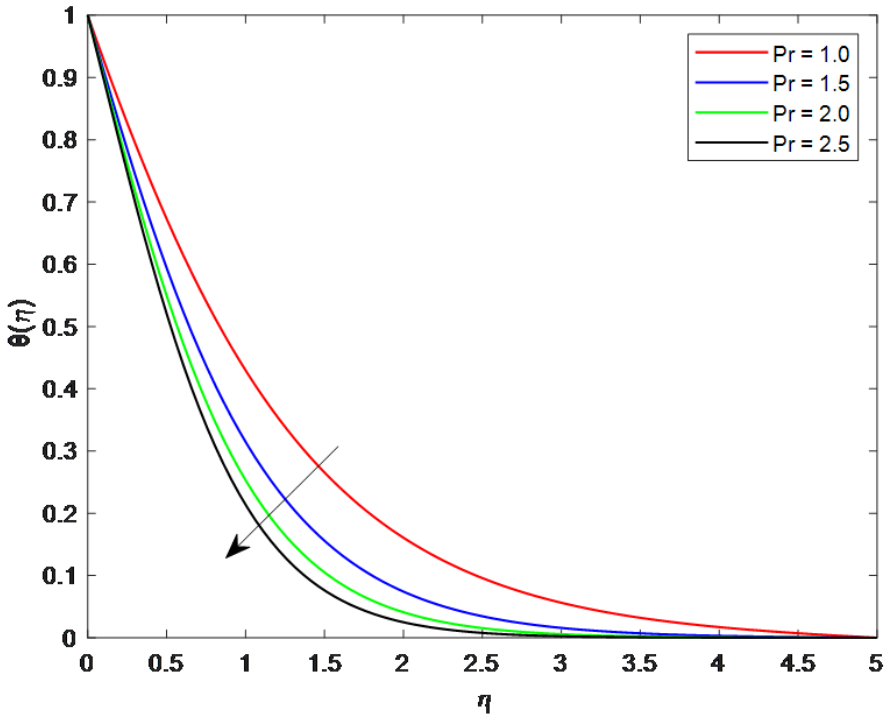

Fig. 5: Temperature profiles $\theta(\eta)$ for various values of Prandtl number Pr, when $Nb = 0.5$, $Nt = 0.5$, $Da = 0.5$, $Sc = 2$, $M = 0.5$, $\lambda = 0.2$, $Q = -0.1$, $Ec = 0.4$, $R = 0.5$, $\theta_w = 1.2$, $\gamma = 2.5$.

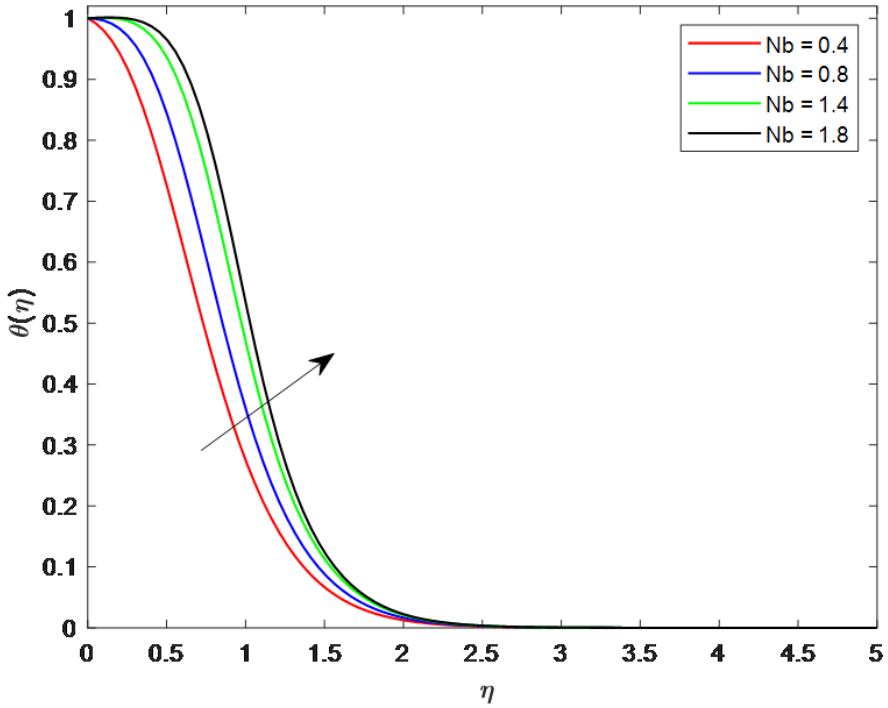

Fig. 6: Temperature profiles $\theta(\eta)$ for various values of Brownian motion parameter Nb, when $Pr = 5$, $Nt = 0.5$, $Da = 0.5$, $Sc = 2$, $M = 0.5$, $\lambda = 0.2$, $Q = -0.1$, $Ec = 0.4$, $R = 0.5$, $\theta_w = 1.2$, $\gamma = 2.5$.

expansion of the Brownian motion parameter leads to an increase in kinetic energy of the particles. This increase in kinetic energy leads to an enhancement of the thermal boundary layer thickness. The influence of the thermophoresis parameter (Nt) on the dimensionless temperature are shown in Fig. 7. It is clearly shown in the figure that thermophoresis parameter has significant effect on the temperature profile. The fact behind this is that the thermophoretic forces is generated by the gradient of temperature which produces a very high-speed flow far from the stretching surface. Considerably the fluid is more heated and away from the stretching sheet, as a result when thermophoresis parameter rises the thermal boundary layer thickness increases. In the presence of viscous dissipation, the effect of Eckert number (Ec) on the temperature profile $\theta(\eta)$ nanofluid is shown in Fig. 8. Here we observed that

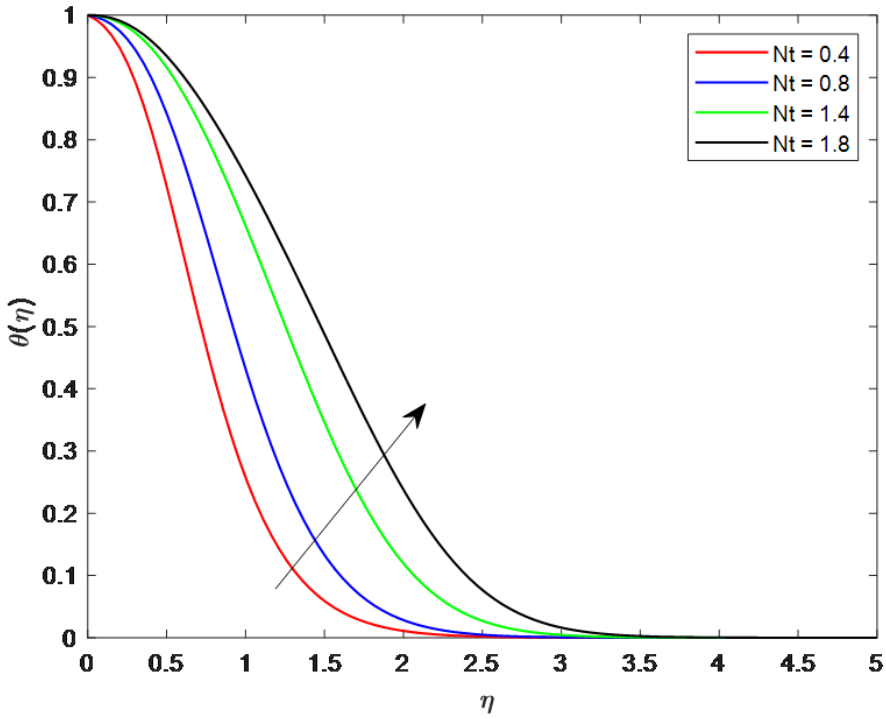

Fig. 7: Temperature profiles $\theta(\eta)$ for various values of thermophoresis parameter Nt , when $Pr = 5$, $Nb = 0.5$, $Da = 0.5$, $Sc = 2$, $M = 0.5$, $\lambda = 0.2$, $Q = -0.1$, $Ec = 0.4$, $R = 0.5$, $\theta_w = 1.2$, $\gamma = 2.5$.

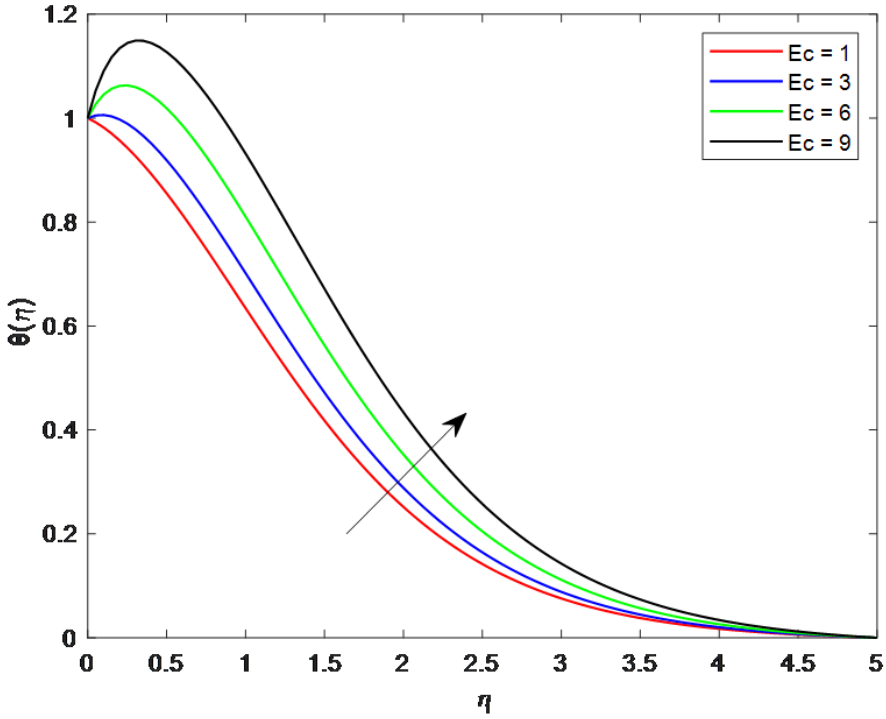

Fig. 8: Temperature profiles $\theta(\eta)$ for various values of Eckert number Ec , when $Pr = 5$, $Nb = 0.5$, $Da = 0.5$, $Sc = 2$, $M = 0.5$, $\lambda = 0.2$, $Q = -0.1$, $Nt = 0.5$, $R = 0.5$, $\theta_w = 1.2$, $\gamma = 2.5$.

with the increase of the Eckert number the temperature profile $\theta(\eta)$ expand along the stretching sheet. This is due to the viscous dissipation effects which is caused by the thermal reversal procedure in the boundary layer near the surface of the stretching. Fig. 9 shows the relation between nonlinear thermal radiation parameter (R) with the temperature profile $\theta(\eta)$. From figure it is observed that the temperature profile increases with increasing value of thermal radiation parameter. The radiation parameter is a measure of the intensity of thermal radiation. When R increases, the intensity of thermal radiation increases, which leads to an increase in the rate of heat transfer. Thus, in turn causes the temperature profile to increase. The impact in the ratio temperature parameter (θ_w) on temperature profile is depicted in Fig. 10. From the figure it is noted that with increase in the ratio temperature parameter

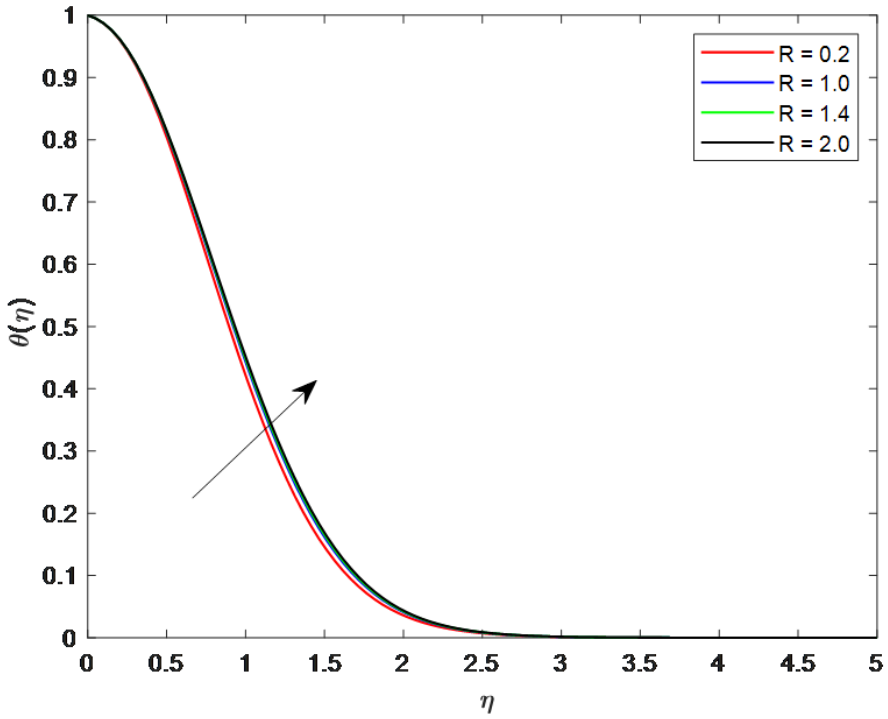

Fig. 9: Temperature profiles $\theta(\eta)$ for various values of radiation parameter R, when $Pr = 5$, $Nb = 0.5$, $Da = 0.5$, $Sc = 2$, $M = 0.5$, $\lambda = 0.2$, $Q = -0.1$, $Nt = 0.5$, $Ec = 0.4$, $\theta_w = 1.2$, $\gamma = 2.5$.

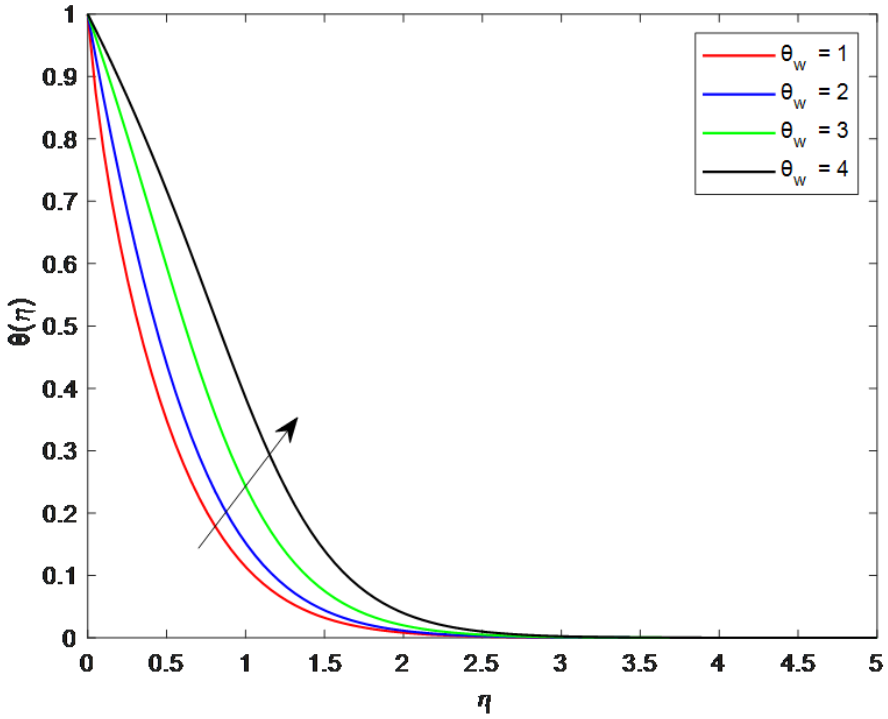

Fig. 10: Temperature profiles $\theta(\eta)$ for various values of ratio temperature parameter θ_w, when $Pr = 5$, $Nb = 0.5$, $Da = 0.5$, $Sc = 2$, $M = 0.5$, $\lambda = 0.2$, $Q = -0.1$, $Nt = 0.5$, $Ec = 0.4$, $R = 0.5$, $\gamma = 2.5$.

the temperature distribution profile increases. The ratio temperature increases the boundary layer temperature and increases its thickness. The effect of heat generation/absorption parameter (Q) on the temperature profile is shown in Fig. 11. There is significant extension in the distribution of the fluid temperature when the values of the heat generation/absorption parameter (Q) increases. It is a physical phenomenon that in case of heat generation ($Q > 0$) there is an enhancement in the transfer and thermal spread of the fluids, which raises temperature of fluid and thickness of the boundary layer. However, an opposite relation occurs in the case of the heat absorption ($Q < 0$). But when moving upward from the state of heat absorption type to the state of heat generation type, there is an improvement in the rate of thermal diffusion and the thickness of the boundary layer.

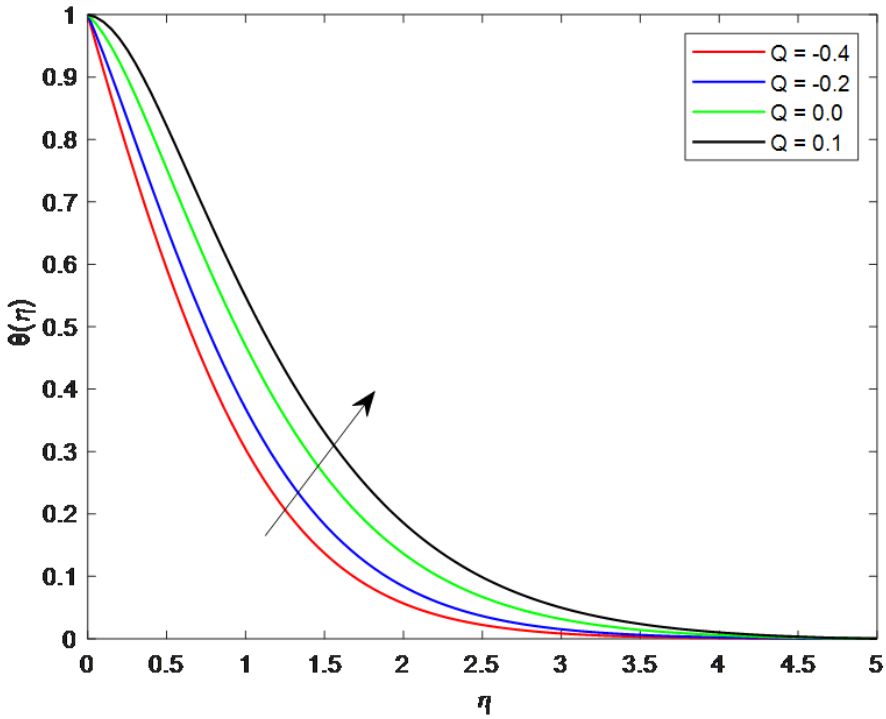

Fig. 11: Temperature profiles $\theta(\eta)$ for various values of heat generation/absorption parameter Q, when $Pr = 5$, $Nb = 0.5$, $Da = 0.5$, $Sc = 2$, $M = 0.5$, $\lambda = 0.2$, $\theta_w = 1.2$, $Nt = 0.5$, $Ec = 0.4$, $R = 0.5$, $\gamma = 2.5$.

4.3 Impact on concentration profile $\phi(\eta)$

The impact of Brownian motion parameter (Nb), on nanoparticle volume fraction $\phi(\eta)$ has been shown in Fig. 12. From figure, we noted that the Brownian motion parameter has inverse behavior with nanoparticle volume fraction. The effect of the Darcy number (Da), on nanoparticle volume fraction $\phi(\eta)$ has been shown in Fig. 13. From figure we find that for the enhancement of Darcy number the nanoparticle volume fraction increases. It is found that there is an opposite relation occurs both in the case of the Schmidt number (Sc) and chemical relation parameter (γ) on the concentration profile which is shown in Fig. 14 and Fig. 15. When describing the ratio of momentum to mass diffusivity, the Schmidt number is utilized. The concentration profile lowers as the Schmidt number rises because a higher Sc value corresponds to a higher chemical molecule diffusivity (smaller values of Scare). A higher Schmidt number consequently results in a significant reduction in the thickness of the concentration boundary layer. The original species that was diffusing in the polymeric viscoelastic fluid is gradually destroyed by a chemical reaction that occurs in a destructive situation. Thus, concentration magnitudes and concentration boundary layer thickness drop as a result of suppressing molecular diffusion of the remaining species.

4.4 Validation of the present outcomes with the existing results in the literature

The results obtained above have been validated numerically by comparing it with the results obtained by Nadeem and Hussain (2014) in the absence of nonlinear thermal radiation, heat generation/absorption, chemical reaction, magnetic and Darcy effects and expressed through Figs. 16, 17 and 18. There is good agreement between the current findings and those of Nadeem and Hussain. Hence the validity and accuracy of the current results have been established.

4.5 Impact on local skin friction C_f, local Nusselt number Nu_x and local Sherwood number Sh_x

The impact of various parameter on the local skin friction coefficient, local Nusselt number and Sherwood number is shown in Tab. 1 and Tab. 2. The local skin friction coefficient decreases with the increasing values of magnetic field parameter (M), radiation parameter (R), Darcy number (Da), Brownian motion parameter (Nb), Schmidt number (Sc), heat generation/absorption parameter (Q), while it increases with increasing values of non-Newtonian Williamson parameter (λ), thermophoresis parameter (Nt), Eckert number (Ec), Prandtl number (Pr), ratio temperature parameter (θ_w). It is also shown that the rate of heat transfer is a decreasing function of the Da, Nb, Nt and Sc. While it increases with increasing value of radiation parameter (R). Sherwood number increases with the increases of the Schmidt number (Sc), chemical reaction parameter (γ) and the thermophoresis parameter (Nt). Whereas the decreasing behavior is shown with Brownian motion parameter (Nb) and non-Newtonian Williamson parameter (λ).

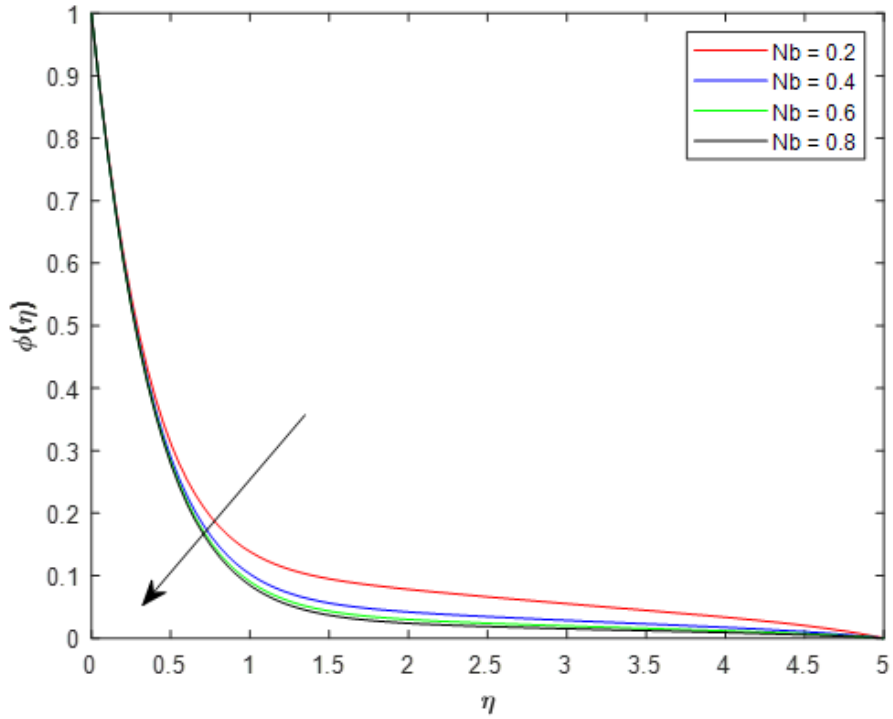

Fig. 12: Concentration of nanoparticle profiles $\phi(\eta)$ for various values of Brownian motion parameter Nb, when $Pr = 5$, $Da = 0.5$, $Q = -0.1$, $Sc = 2$, $M = 0.5$, $\lambda = 0.2$, $\theta_w = 1.2$, $Nt = 0.5$, $Ec = 0.4$, $R = 0.5$, $\gamma = 2.5$.

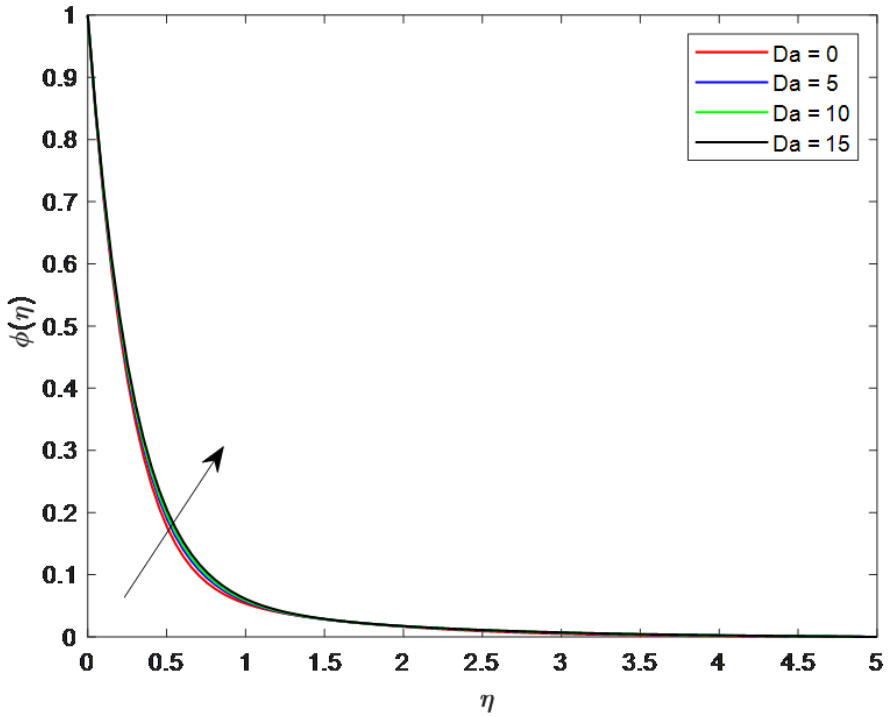

Fig. 13: Concentration of nanoparticle profiles $\phi(\eta)$ for various values of Darcy number Da, when $Pr = 5$, $Nt = 0.5$, $Q = -0.1$, $Sc = 2$, $M = 0.5$, $\lambda = 0.2$, $\theta_w = 1.2$, $Nb = 0.5$, $Ec = 0.4$, $R = 0.5$, $\gamma = 2.5$.

5 Conclusions

The present research work analyzes the nonlinear thermal radiation heat generation/absorption and chemical reaction effects on hydromagnetic Williamson nanofluid flow over a stretching sheet. The important findings of the paper are as follows:

- The velocity distribution $f'(\eta)$ of the fluid is negatively affected by the impact of magnetic field parameter (M), non-Newtonian Williamson parameter (λ) and the Darcy number (Da).
- The enhacement in the value of the radiation parameter (R), the ratio tempetuure parameter (θ_w), the heat genera-

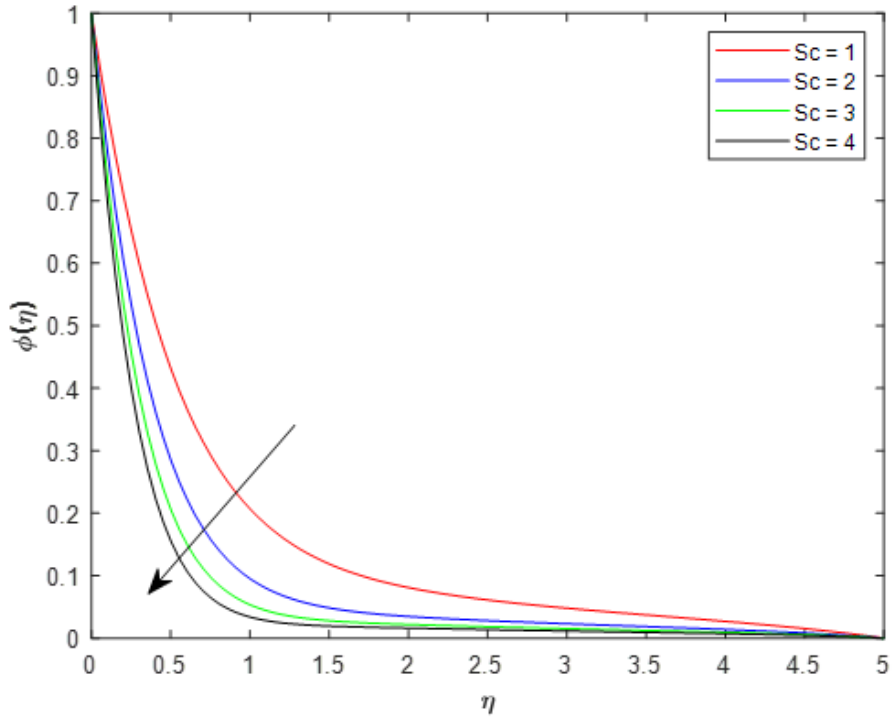

Fig. 14: Concentration of nanoparticle profiles $\phi(\eta)$ for various values of Schmidt number Sc, when $Pr = 5$, $Nt = 0.5$, $Q = -0.1$, $Da = 0.4$, $M = 0.5$, $\lambda = 0.2$, $\theta_w = 1.2$, $Nb = 0.5$, $Ec = 0.4$, $R = 0.5$, $\gamma = 2.5$.

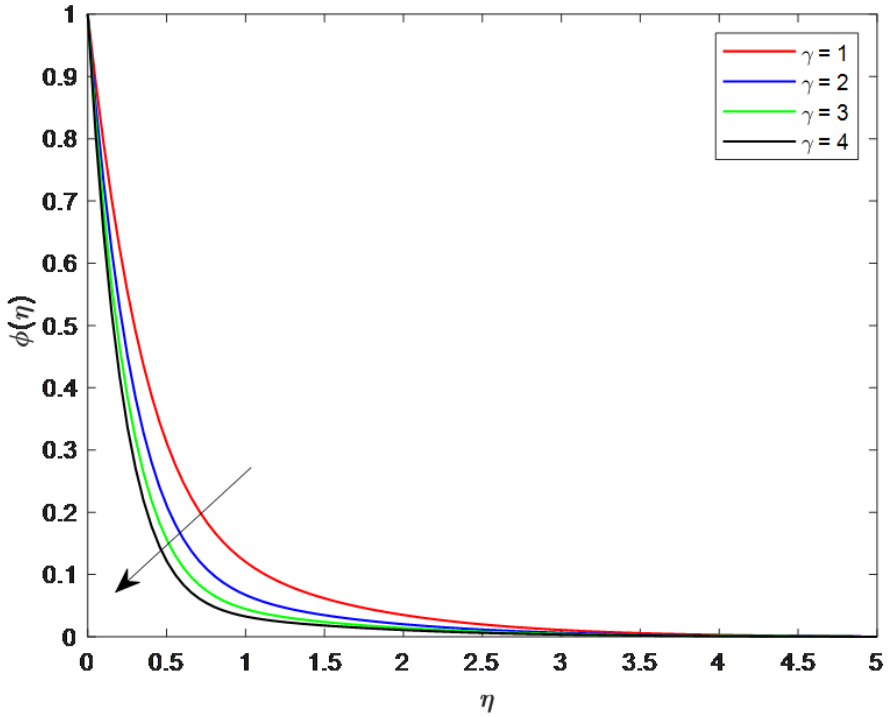

Fig. 15: Concentration of nanoparticle profiles $\phi(\eta)$ for various values of chemical reaction parameter γ, when $Pr = 5$, $Nt = 0.5$, $Q = -0.1$, $Da = 0.4$, $M = 0.5$, $\lambda = 0.2$, $\theta_w = 1.2$, $Nb = 0.5$, $Ec = 0.4$, $R = 0.5$, $Sc = 2$.

tion/absorption parameter (Q), darcy number (Da) and the Eckert number (Ec) resulted in the enhancement of temperature distribution $\theta(\eta)$ of the fluid.

- It is found that the distribution of the concentration of nanoparticles $\phi(\eta)$ decreases under the influence of Brownian motion parameter (Nb), Schmidt number (Sc) and chemical reaction parameter (γ).
- It is found that the enhancement of the values of thermophoresis parameter (Nt) resulted in the enhancement in the distributions of temperature $\theta(\eta)$ profile.
- The distribution of the concentration of nanoparticles $\phi(\eta)$ increases with increasing value of the Darcy number (Da).

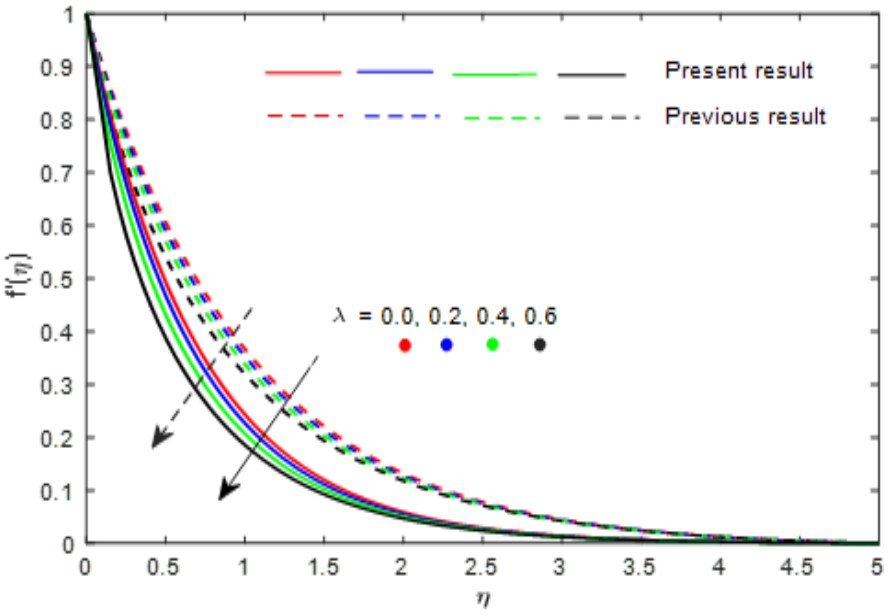

Fig. 16: Velocity profiles $f'(\eta)$ for various values of non-Newtonian Williamson parameter λ, when $Pr = 5$, $Nt = 0.5$, $Nb = 0.5$, $Q = 0$, $Da = 0$, $M = 0$, $\gamma = 0$, $\theta_w = 0$, $Ec = 0$, $R = 0$, $Sc = 2$.

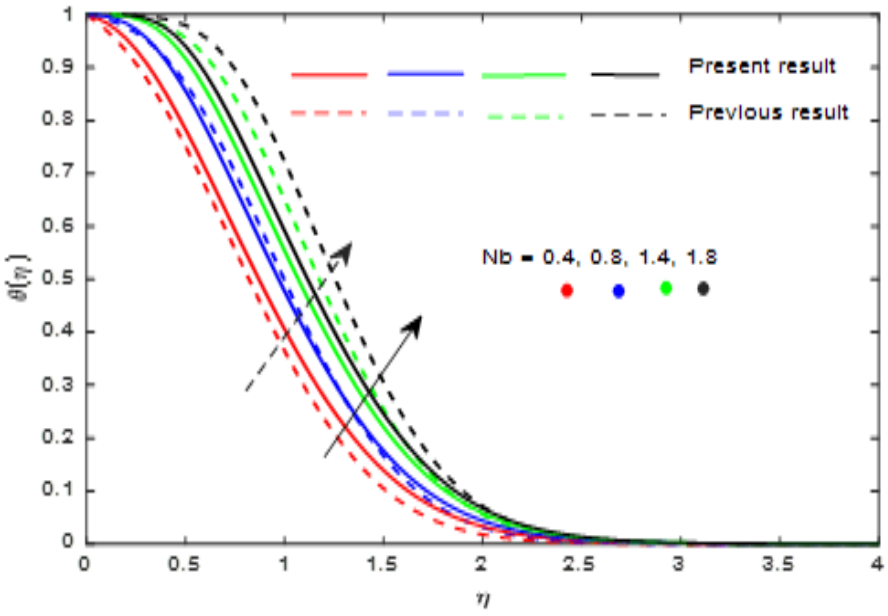

Fig. 17: Temperature profiles $\theta(\eta)$ for various values of the Brownian motion parameter Nb, when $Pr = 5$, $Nt = 0.5$, $\lambda = 0.2$, $Q = 0$, $Da = 0$, $M = 0$, $\gamma = 0$, $\theta_w = 0$, $Ec = 0$, $R = 0$, $Sc = 2$.

- The local skin friction coefficient has an inverse effect with the M,R,Da and Nb, while it is directly propertional to the value of non-Newtonian Williamson parameter (λ), thermophoresis parameter (Nt), Eckert number (Ec), Prandtl number (Pr), ratio temperature parameter (θ_w).
- The rate of heat transfer is a decreasing function of the Da, Nb, Nt and Sc, while it increases with increasing value of radiation parameter R.
- The rate of mass transfer is increasing function of Schmidt number (Sc) and chemical reaction parameter (γ), while it has inverse effect with the Brownian motion parameter (Nb) and the thermophoresis parameter (Nt).

References

K. Ahmed, T. Akbar, T. Muhammad, and M. Alghamdi. Heat transfer characteristics of mhd flow of williamson nanofluid over an exponential permeable stretching curved surface with variable thermal conductivity. *Case Studies in Thermal Engineering*, 28: 101544, 2021. doi: https://doi.org/10.1016/j.csite.2021.101544.

Hamid, H. Aamir, and M. Khan. Multiple solutions for MHD transient flow of williamson nanofluids with convective heat transport.

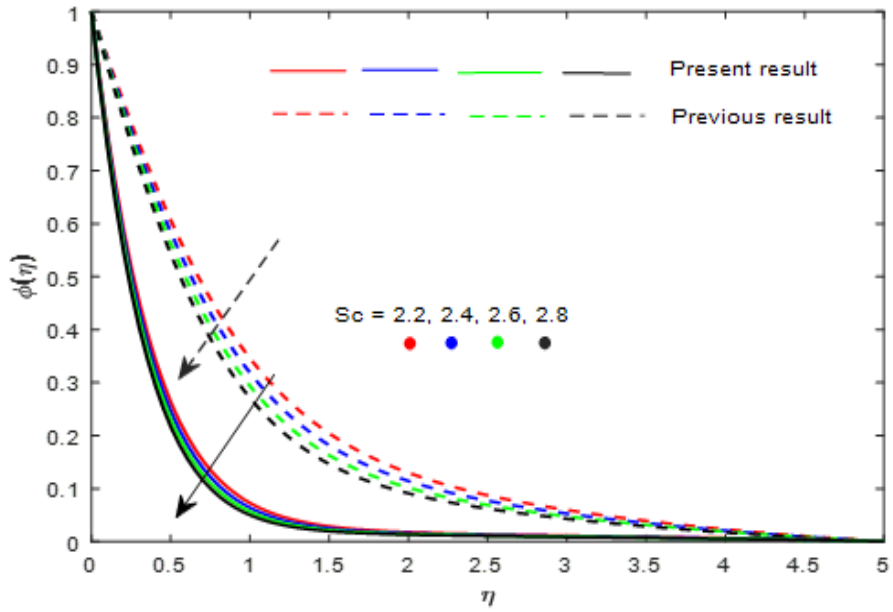

Fig. 18: Concentration of nanoparticle profiles $\theta(\eta)$ for various values of Schmidt number Sc, when $Pr = 5$, $Nt = 0.5$, $\lambda = 0.2$, $Q = 0$, $Da = 0$, $M = 0$, $\gamma = 0$, $\theta_w = 0$, $Ec = 0$, $R = 0$, $Nb = 0.5$.

Tab. 1: Numerical value for local Skin friction coefficient, Nusselt number and Sherwood number with relevent parameters.

M	R	Da	λ	Nb	Nt	$\sqrt{Re_x}C_f$	$\frac{Nu_x}{\sqrt{Re_x}}$	$\frac{Sh_x}{\sqrt{Re_x}}$
0.1	0.5	0.5	0.2	0.5	0.5	-1.202704099	0.487905223	1.442844324
0.3						-1.271583704	0.377558219	1.483812600
0.6						-1.367162498	0.219523738	1.543641532
0.5	0.1	0.5	0.2	0.5	0.5	-1.336232419	0.168144293	1.601493091
	0.4					-1.336232400	0.245415296	1.537605233
	0.8					-1.336232354	0.002615688	1.656110861
0.5	0.5	1	0.2	0.5	0.5	-1.482961595	0.021051829	1.620467540
		2				-1.730518709	0.047736826	1.585019604
		3				-1.936420538	0.067672109	1.557068247
0.5	0.5	0.5	0.2	0.5	0.5	-1.336232353	0.002996860	1.643061950
			0.3			-1.287762979	0.012499776	1.633225882
			0.4			-1.224013613	0.027514439	1.618224716
0.5	0.5	0.5	0.2	0.1	0.5	-1.336232212	0.549269494	1.829228158
				0.2		-1.336232352	0.359705932	1.774318470
				0.3		-1.336232353	0.209115313	1.725619901
0.5	0.5	0.5	0.2	0.5	0.1	-1.336232427	0.240225803	1.367102707
					0.3	-1.336232403	0.099304135	1.499584035
					0.4	-1.336232401	0.046628857	1.570967824

Journal of the Taiwan Institute of Chemical Engineers, 103:126–137, 2019. doi: https://doi.org/10.1016/j.jtice.2019.07.001.

T. Hayat, M. Z. Kiyani, A. Alsaedi, M. I. Khan, and I. Ahmad. Mixed convective three-dimensional flow of williamson nanofluid subject to chemical reaction. *International Journal of Heat and Mass Transfer*, 127:422–429, 2018. doi: https://doi.org/10.1016/j.ijheatmasstransfer.2018.06.124.

A. Hussain, M. Y. Malik, T. Salahuddin, S. Bilal, and M. Awais. Combined effects of viscous dissipation and joule heating on MHD sisko nanofluid over a stretching cylinder. *Journal of Molecular Liquids*, 231:341–352, 2017. doi: https://doi.org/10.1016/j.molliq.2017.02.030.

M. M. Khader, M. M. Babatin, and A. M. Megahed. Numerical simulation by using the spectral collocation method for williamson nanofluid flow over an exponentially stretching sheet with slip velocity. *Journal of Nonlinear Mathematical Physics*, 30(3): 1134–1152, 2023. doi: https://doi.org/10.1007/s44198-023-00115-7.

M. Khan, T. Salahuddin, M. Y. Malik, and F. O. Mallawi. Change in viscosity of williamson nanofluid flow due to thermal and solutal stratification. *International Journal of Heat and Mass Transfer*, 126:941–948, 2018. doi: https://doi.org/10.1016/j.ijheatmasstransfer.2018.05.074.

W. A. Khan and I. Pop. Boundary-layer flow of a nanofluid past a stretching sheet. *International journal of heat and mass transfer*, 53(11-12):2477–2483, 2010. doi: https://doi.org/10.1016/j.ijheatmasstransfer.2010.01.032.

Tab. 2: Numerical value for local Skin friction coefficient, Nusselt number and Sherwood number with relevent parameters.

Pr	Sc	Q	Ec	θ_w	γ	$\sqrt{Re_x}C_f$	$\frac{Nu_x}{\sqrt{Re_x}}$	$\frac{Sh_x}{\sqrt{Re_x}}$
1	2	-0.1	0.4	1.2	0.6	-1.336232430	0.439986907	1.397948145
3						-1.336232422	0.360440338	1.462175700
5						-1.336232419	0.236705206	1.530735820
5	1	-0.1	0.4	1.2	0.6	-1.336232355	0.135458703	1.103887560
	1.5					-1.336232354	0.048706439	1.407364660
	2					-1.336232353	0.002996860	1.643061950
5	2	-0.4	0.4	1.2	0.6	-1.336232424	0.629322117	1.379693200
		-0.3				-1.336232400	0.438859517	1.463923655
		-0.1				-1.336232353	0.002996860	1.643061950
5	2	-0.1	0.3	1.2	0.6	-1.336232399	0.337358742	1.494178813
			0.6			-1.336232354	0.137932005	1.583438194
			0.8			-1.336232353	0.002996860	1.643061950
5	2	-0.1	0.4	1.1	0.6	-1.336232402	0.240065395	1.581049401
				1.3		-1.336232353	0.307971996	1.466806441
				1.5		-1.336232204	0.400190281	1.357479584
5	2	-0.1	0.4	1.2	0.5	-1.336232353	0.292924510	1.417095460
					1.5	-1.336232400	0.177134333	2.198082605
					2.5	-1.336232353	0.139125263	2.698543198

R. M. Kumar, R. S. Raju, F. Mebarek-Oudina, M. A. Kumar, and V. K. Narla. Cross-diffusion effects on an mhd williamson nanofluid flow past a nonlinear stretching sheet immersed in a permeable medium. *Frontiers in Heat and Mass Transfer*, 22(1): 15–34, 2024. doi: http://dx.doi.org/10.32604/fhmt.2024.048045.

A. V. Kuznetsov and D. A. Nield. Natural convective boundary-layer flow of a nanofluid past a vertical plate. *International Journal of Thermal Sciences*, 49(2):243–247, 2010. doi: https://doi.org/10.1016/j.ijthermalsci.2009.07.015.

S. Nadeem and S. T. Hussain. Flow and heat transfer analysis of williamson nanofluid. *Applied Nanoscience*, 4:1005–1012, 2014. doi: https://doi.org/10.1007/s13204-013-0282-1.

S. Nadeem, S. T. Hussain, and C. Lee. Flow of a williamson fluid over a stretching sheet. *Brazilian journal of chemical engineering*, 30:619–625, 2013. doi: https://doi.org/10.1590/S0104-66322013000300019.

C. S. K. Raju, N. Sandeep, and A. Malvandi. Free convective heat and mass transfer of MHD non-newtonian nanofluids over a cone in the presence of non-uniform heat source/sink. *Journal of Molecular Liquids*, 221:108–115, 2016. doi: https://doi.org/10.1016/j.molliq.2016.05.078.

G. K. Ramesh, B. J. Gireesha, and C. S. Bagewadi. Heat transfer in MHD dusty boundary layer flow over an inclined stretching sheet with non-uniform heat source/sink. *Advances in Mathematical Physics*, 2012(6):1–13, 2012. doi: https://doi.org/10.1155/2012/657805.

S. Rao and P. N. Deka. Numerical analysis of mhd hybrid nanofluid flow a porous stretching sheet with thermal radiation. *International Journal of Applied and Computational Mathematics*, 10(3):95, 2024. doi: http://dx.doi.org/10.1007/s40819-024-01734-4.

S. A. Sajadifar, A. Karimipour, and D. Toghraie. Fluid flow and heat transfer of non-newtonian nanofluid in a microtube considering slip velocity and temperature jump boundary conditions. *European Journal of Mechanics-B/Fluids*, 61:25–32, 2017. doi: https://doi.org/10.1016/j.euromechflu.2016.09.014.

M. Sheikholeslami and D. D. Ganji. Three dimensional heat and mass transfer in a rotating system using nanofluid. *Powder Technology*, 253:789–796, 2014. doi: https://doi.org/10.1016/j.powtec.2013.12.042.

K. Subbarayudu, S. Suneetha, and P. B. A. Reddy. The assessment of time dependent flow of williamson fluid with radiative blood flow against a wedge. *Propulsion and Power Research*, 9(1):87–99, 2020. doi: https://doi.org/10.1016/j.jppr.2019.07.001.

R. V. Williamson. The flow of pseudoplastic materials. *Industrial & Engineering Chemistry*, 21(11):1108–1111, 1929. doi: https://doi.org/10.1021/ie50239a035.

N. S. Yousef, A. M. Megahed, N. I. Ghoneim, M. Elsafi, and E. Fares. Chemical reaction impact on mhd dissipative casson-williamson nanofluid flow over a slippery stretching sheet through porous medium. *Alexandria Engineering Journal*, 61(12): 10161–10170, 2022. doi: http://dx.doi.org/10.1016/j.aej.2022.03.032.